Phase-retrieval Effect on Angiographic X-ray Imaging

Simón González López

Advisor: Carlos A. Ávila Bernal, PhD

Universidad de los Andes | Grupo de Investigación Altas Energías

Motivation: Angiography

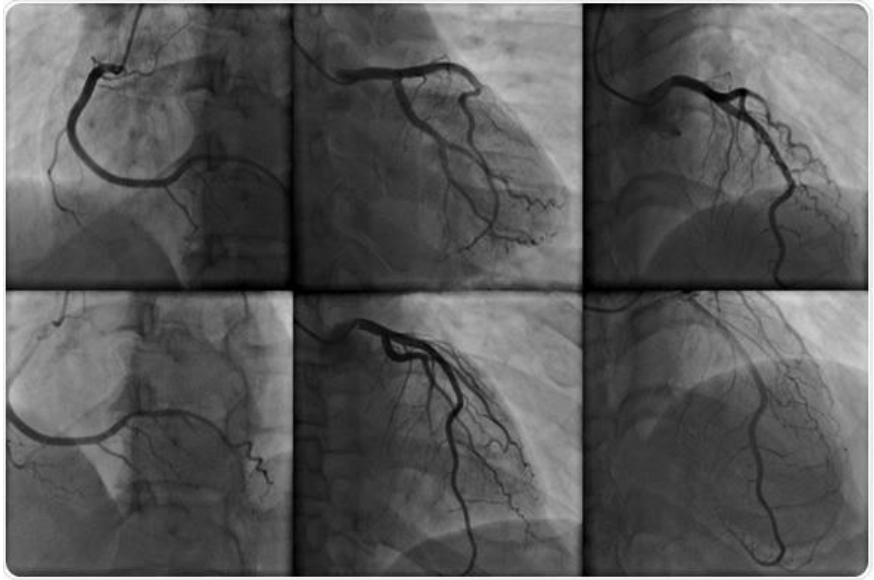

Fig 1. Angiography procedure. Taken from [1].

- **Invasive method.**
- Blood vessels can't absorb well X-rays [2].
- Low contrast imaging.
- No visibility of blood vessels' internal walls.
- Requires a contrast agent.

Universidad de los Andes | Grupo de Investigación Altas Energías

Motivation: Atherosclerosis

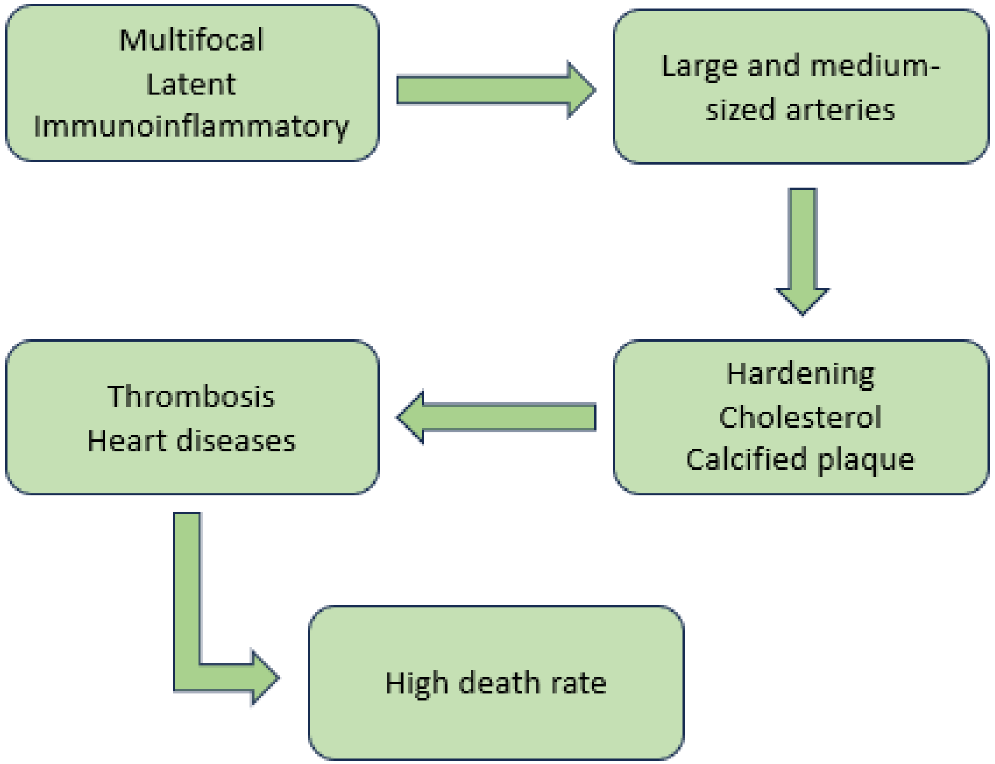

Fig 2. Atherosclerosis disease [3-5].

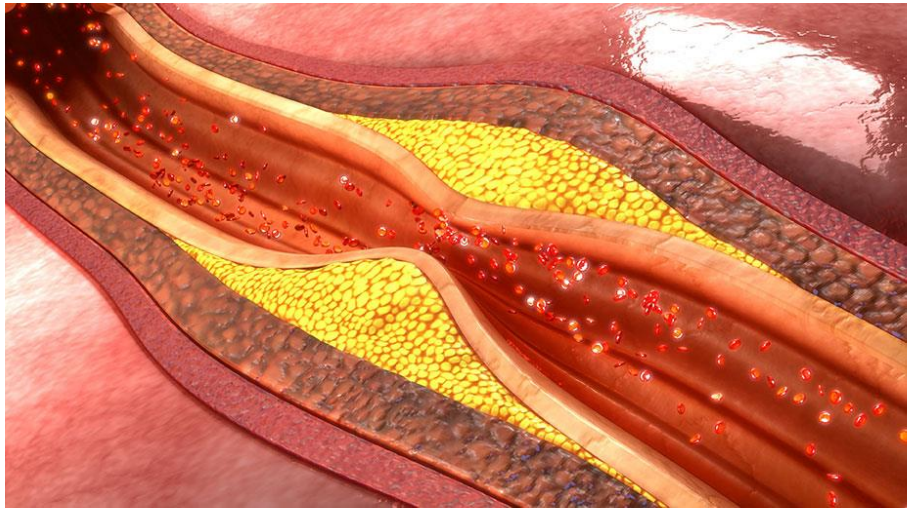

Fig 3. Atherosclerosis disease. Taken from [6].

The objective of our project

- Quantify the phase-retrieval effect in the quality of angiographic images.

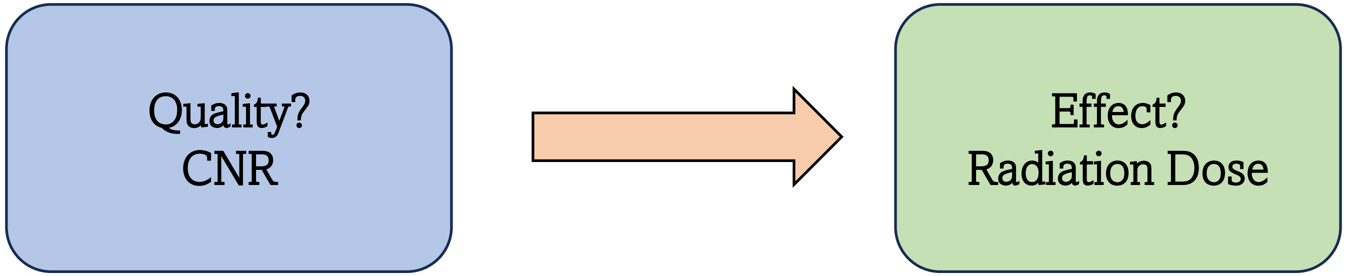

- Compare the techniques of *In-line Phase-contrast Imaging* and *Speckle-based Phase-contrast Imaging.*

A brief theory review

- In-line Phase-contrast Imaging [7-11]

$$I(x_1,y_1) = \frac{I(x,y)}{M^2}\left[1 - \frac{z_1}{kM}\nabla_T^2\Delta\phi(x,y)\right] \qquad M = \frac{z_0+z_1}{z_0}$$

Paganin Algorithm [12]

$$\Delta\phi(x,y,z_0) = \frac{\delta}{2\beta}Ln\left(\mathcal{F}^{-1}\left[\frac{\mathcal{F}(I(x,y,z_1)/I_0)}{1+\frac{z_1\delta}{2k\beta}(k_x^2+k_y^2)}\right]\right)$$

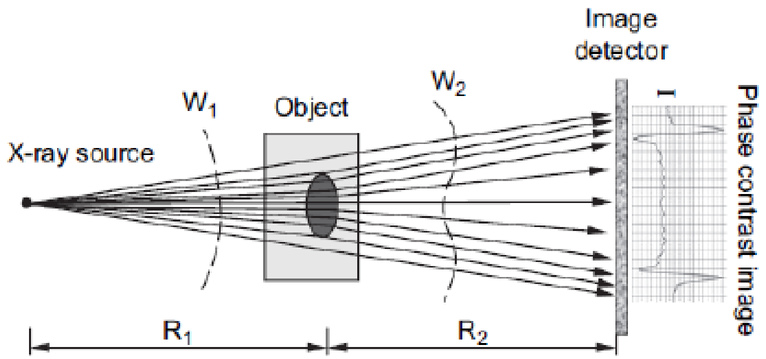

Fig 4. In-line PCI. Taken from [13].

- Speckle Phase-contrast Imaging [14-19]

$$I_R(x,y) - I_M(x,y) = \frac{z_1}{k}\vec{\nabla}_T \cdot \left(I_R(x,y)\vec{\nabla}_T\Delta\phi(x,y)\right) - z_1\nabla_T^2\left(D_{ef}(x,y,z_1)I_R(x,y)\right)$$

MIST Algorithm [20,21]

$$\Delta\phi(x,y) = \frac{\delta}{2\beta}Ln\left(\mathcal{F}^{-1}\left[\frac{\mathcal{F}(\mathcal{S}(x,y))}{1+\frac{2z_1\delta\pi^2}{k\beta}(k_x^2+k_y^2)}\right]\right)$$

$$D_{ef}(x,y,z_1) = \frac{1}{z_1}\frac{I_{M_1}(x,y)I_{R_2}(x,y) - I_{M_2}(x,y)I_{R_1}(x,y)}{I_{R_2}(x,y)\nabla_T^2 I_{R_1}(x,y) - I_{R_1}(x,y)\nabla_T^2 I_{R_2}(x,y)}$$

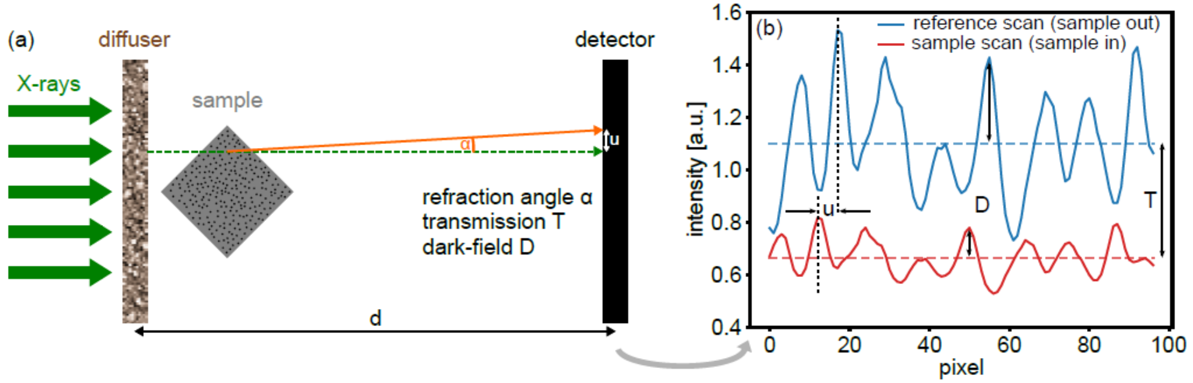

Fig 5. Speckle PCI. Taken from [15].

Metodology

Computational simulations using Geant4 → Experimental images → CNR and absorbed dose calculation → Comparing techniques

Computational simulations using Geant4

- PEPI Package.
- In-line and Speckle-based Phase-contrast imaging for angiography setup design.
- Phase-retrieval.

Experimental images

- In-line and Speckle-based Phase-contrast imaging for angiography setup implementation.
- Inorganic Phantom: PMMA and Organic: Pig artery.
- Phase-retrieval.

CNR and absorbed dose calculation

- CNR calculation to evaluate the angiographic images quality.
- Estimate the absorbed dose to quantify the phase-retrieval effect.

Comparing techniques

- Study which technique provides better quality as a function of the absorbed dose.
- Compare experimental and computational results.

Materials and Methods

- Policromatic X-ray source with $200\mu m$ berilium window: 28kV, 48kV, 78kV.
- Photon-counting detector with silicon sensor and a pixel size of $55\mu m \times 55\mu m$.
- Angiographic phantom made of PMMA/Pig Artery with artificial blood and atherosclerotic plaque HA-PMMA (5%-95%).
- Geometric magnification 2x.

- Additionally for speckle: A sand paper with speck size of $58.5\mu m$ located between the X-ray source and the sample.

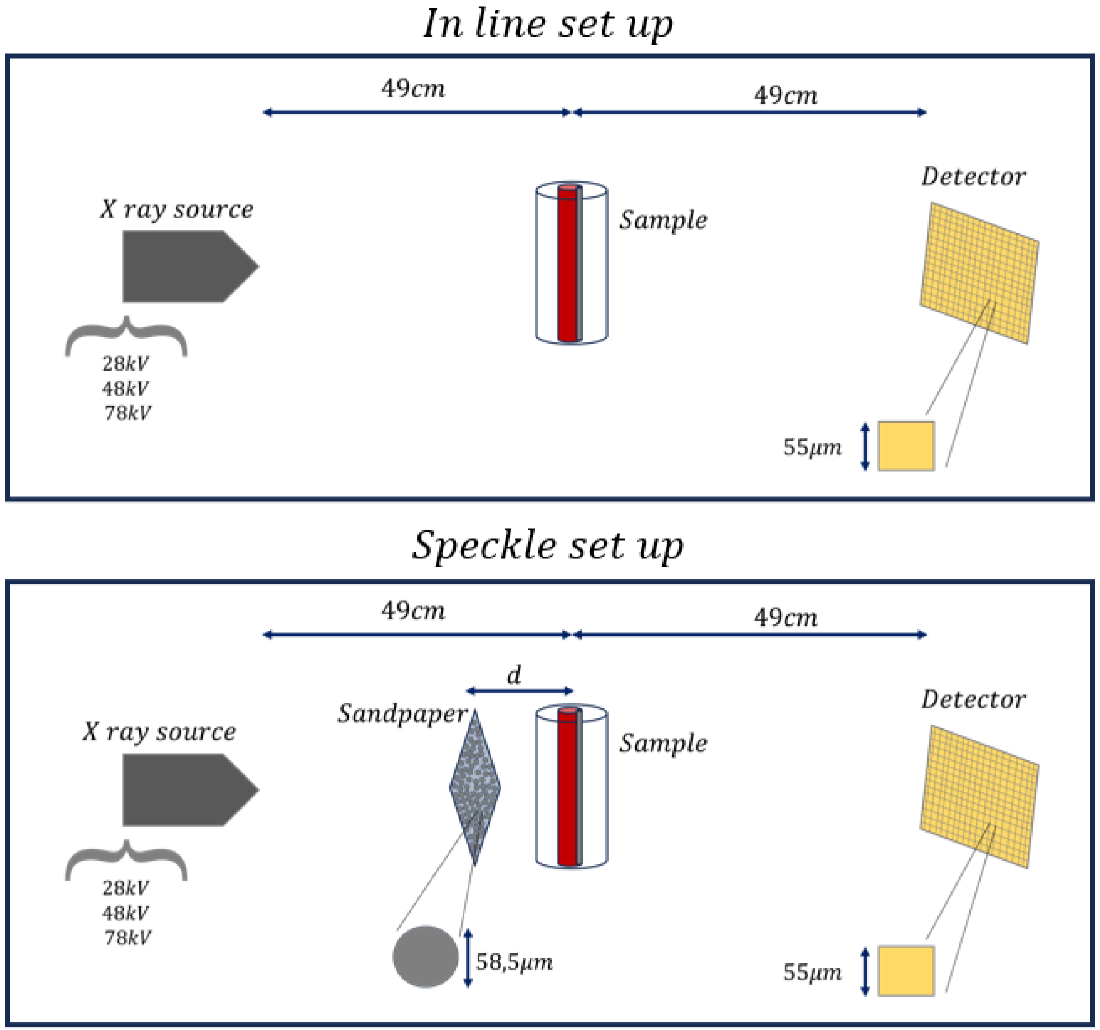

Universidad de los Andes | Grupo de Investigación Altas Energías

Computational Simulations

- Simulations developed in Geant4 [22] using PEPI [23].
- Monte Carlo-based: We use an X-ray spectrum (Fluence vs Energy) [24,25].
- Plaque simulated as a 1/8 of a cylinder inside other one made of PMMA.
- Sandpaper: 2.0×10^5 spheres made of silicon carbide resting on both sides of a cellulose surface of $250\mu m$. Cross steps of $60\mu m$.
- Events: 2×10^9 *raw* y 3×10^9 *flat field*.

In line Simulations

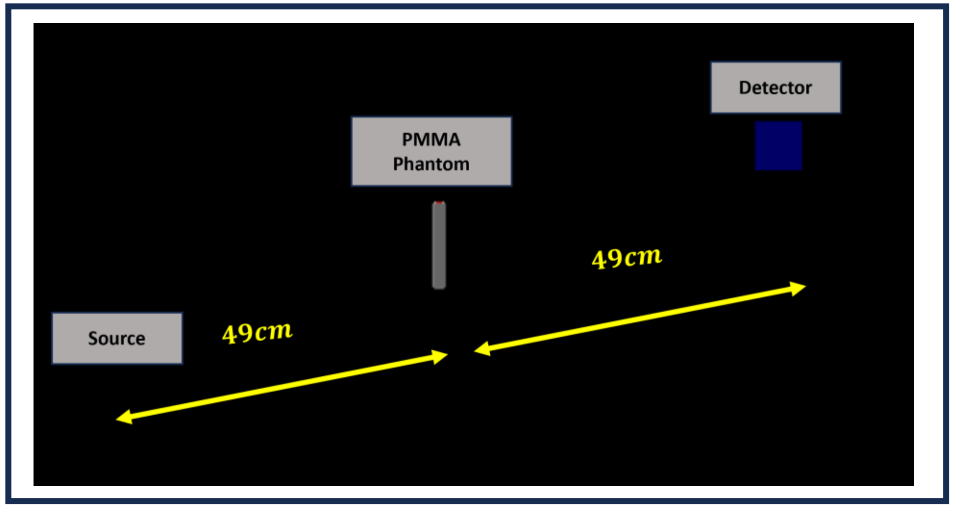

Speckle Simulations

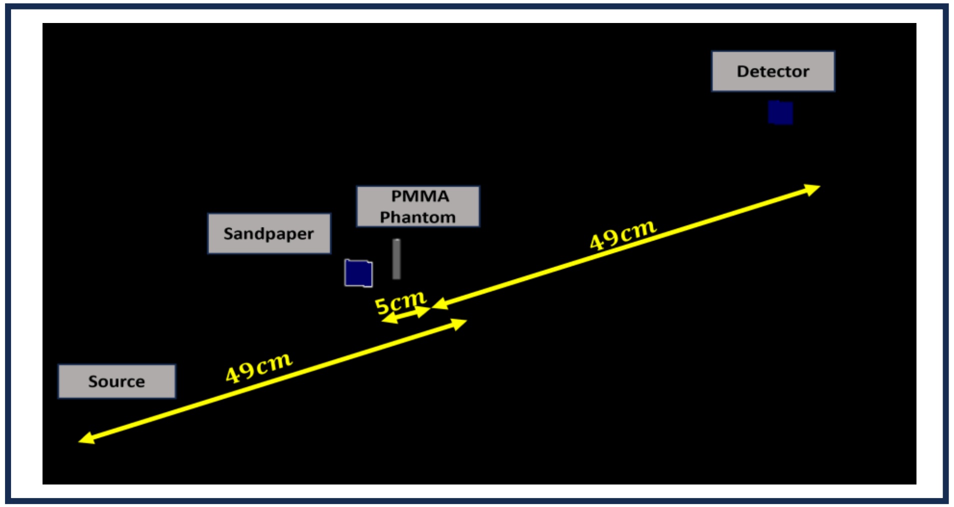

Experimental set up

PMMA Phantom

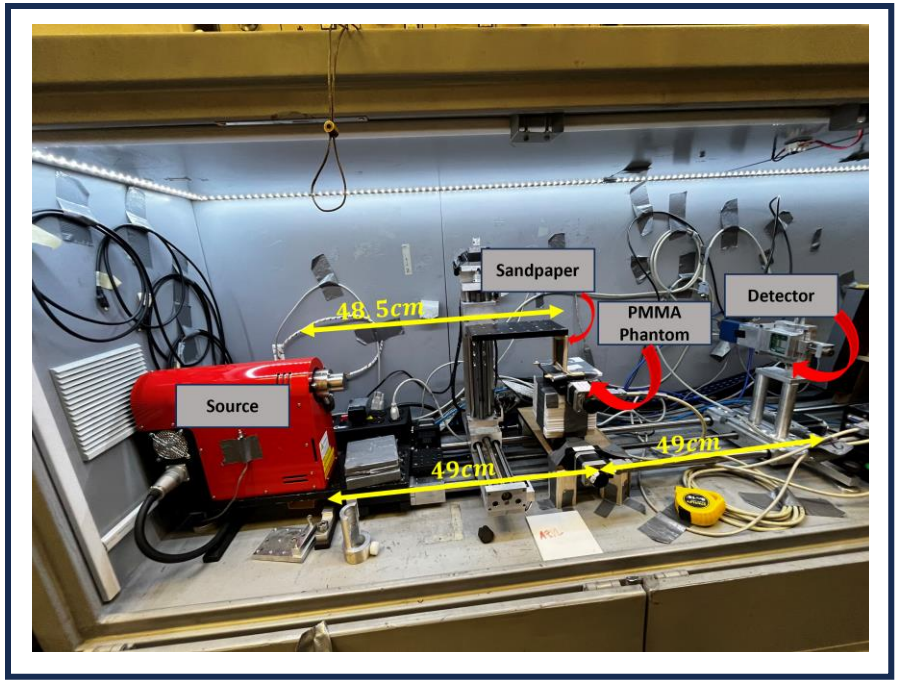

Pig Artery

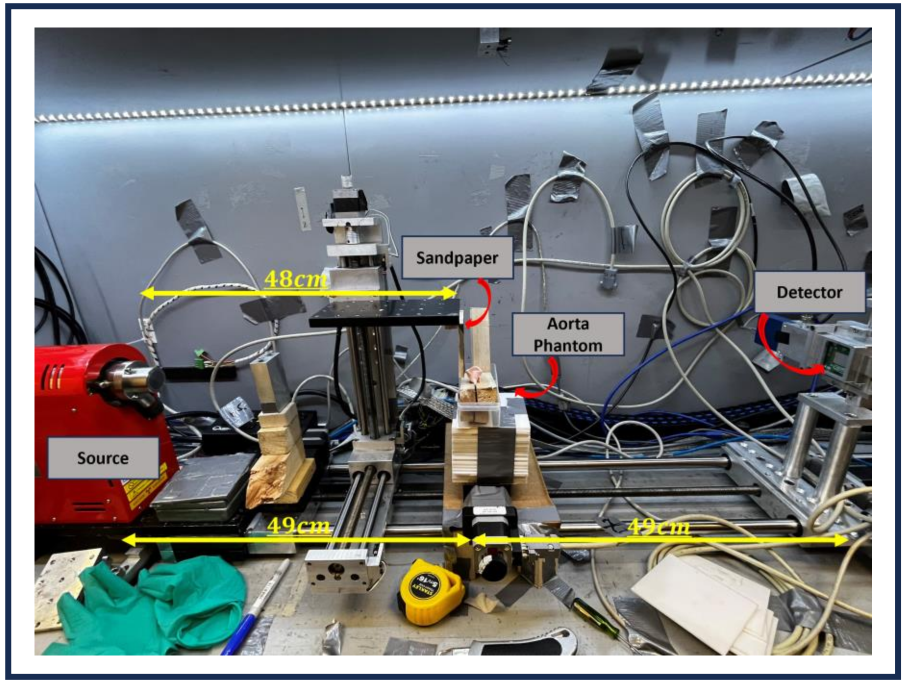

- X-ray source Hammamatsu L6622-01.
- Medipix3RXV1 with silicon sensor detector.

- For Speckle: Sandpaper P240.
- Cross steps of $60\mu m$.

Absorbed dose: Computational Measurement

Dosis absorbida		
Voltaje	Propagación (± 0.02 mGy)	Moteo (± 0.01mGy)
28kV	1.76	0.94
48kV	1.59	0.90
78kV	1.29	0.75

→ In-line provides 1.78 times more absorbed dose than speckle-based. Which means that one phase image retrieved by MIST implies near 12% more absorbed dose than one retrieved by Paganin algorithm.

Computational Results

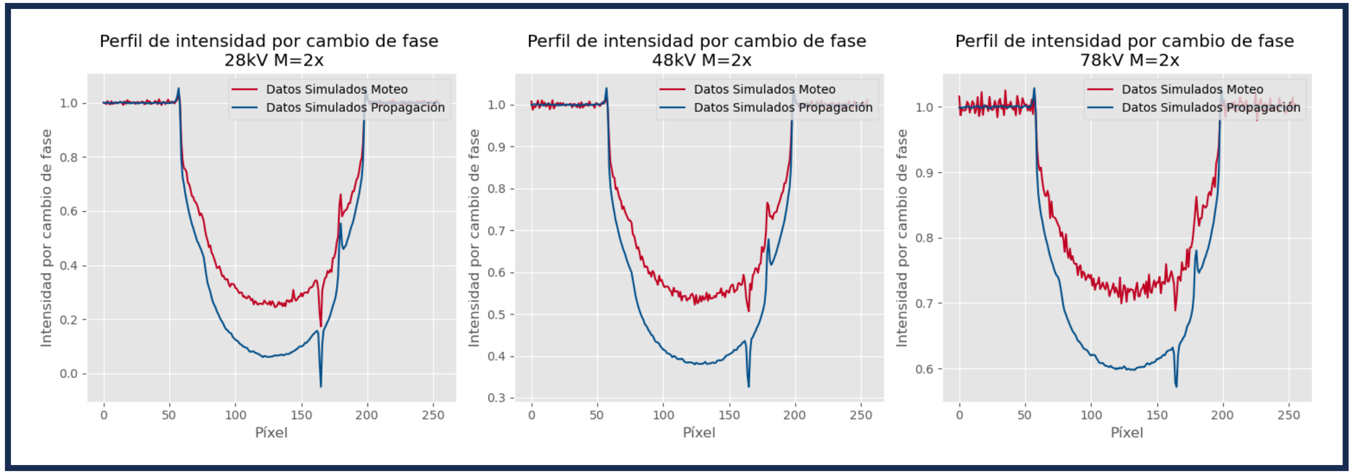

→ It is necesary to apply a Gaussian filter with 150 sigmas to reduce noise in the images

CNR Calculation

CNR imágenes filtradas	
Voltaje	Simulaciones por propagación
28kV	1.396 ± 0.003
48kV	1.426 ± 0.001
78kV	1.457 ± 0.001

CNR imágenes filtradas	
Voltaje	Simulaciones por moteo
28kV	1.33 ± 0.04
48kV	1.29 ± 0.06
78kV	1.2 ± 0.1

Computational Results

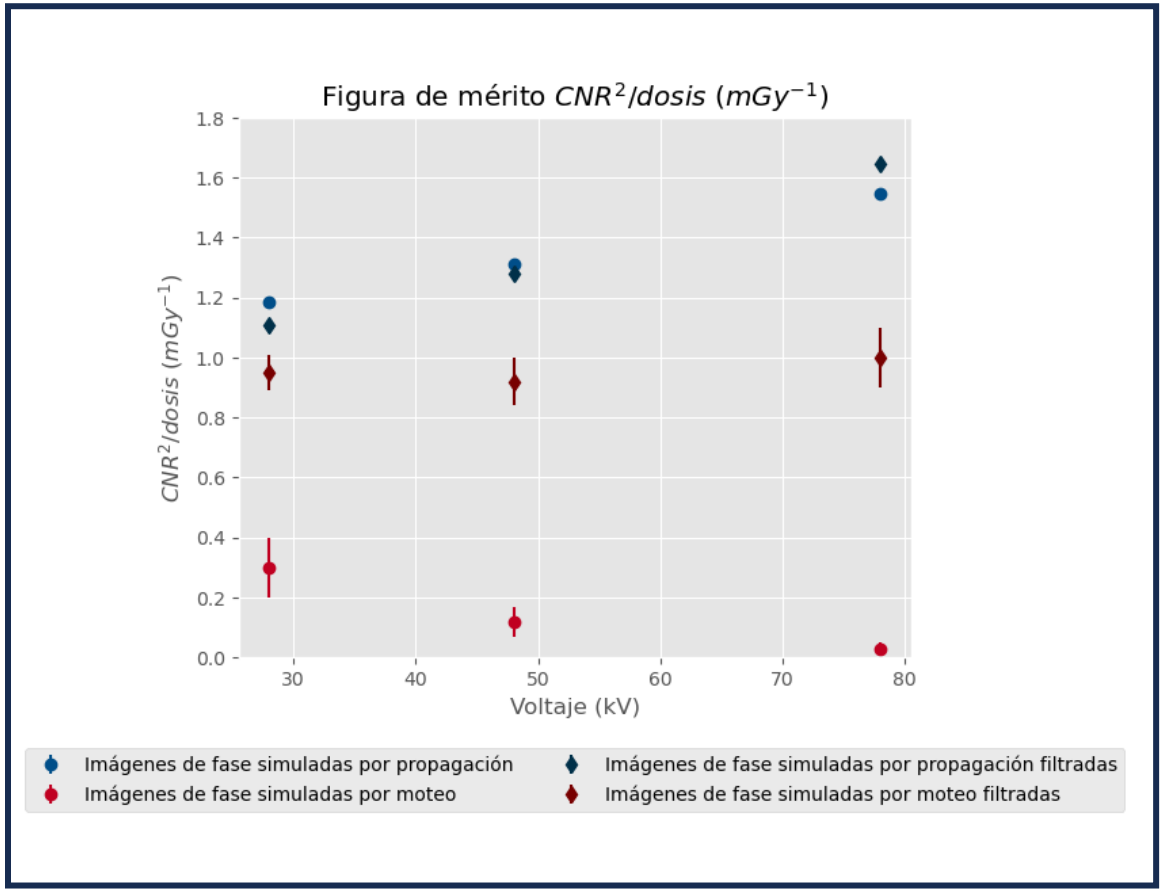

Figura de mérito $CNR^2/dosis\ (mGy^{-1})$				
Voltaje	Propagación	Moteo	Propagación filtrada	Moteo filtrada
28kV	1.185 ± 0.003	0.3 ± 0.1	1.107 ± 0.003	0.95 ± 0.06
48kV	1.311 ± 0.002	0.12 ± 0.05	1.279 ± 0.002	0.92 ± 0.08
78kV	1.548 ± 0.003	0.03 ± 0.02	1.646 ± 0.003	1.0 ± 0.1

In-line provides more visibility per dose absorbed than speckle.
25% at 28kV
42% at 48kV
55% at 78kV

Experimental results: PMMA Phantom

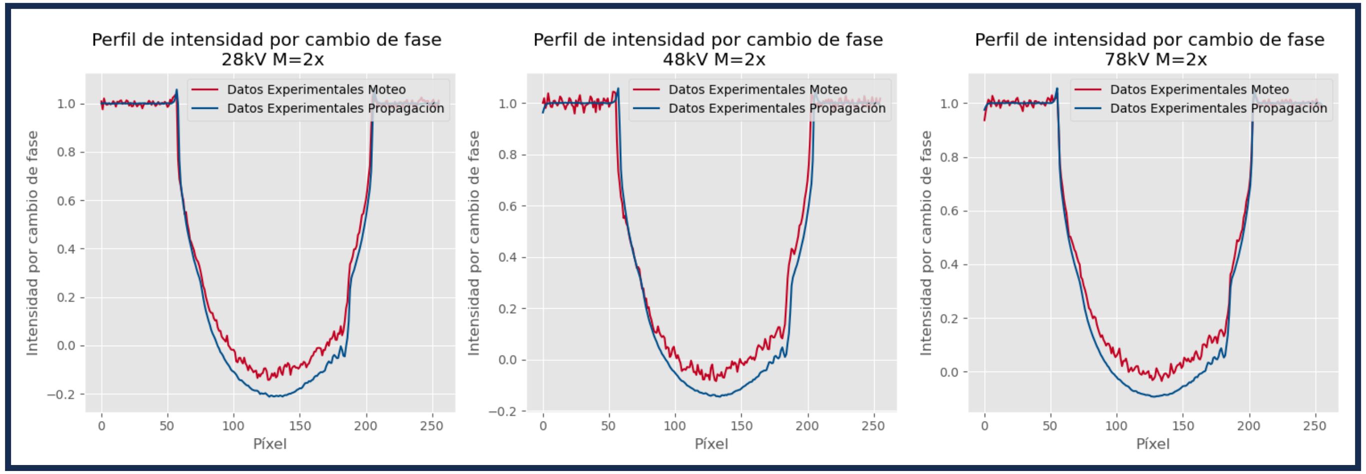

Gaussian Filter

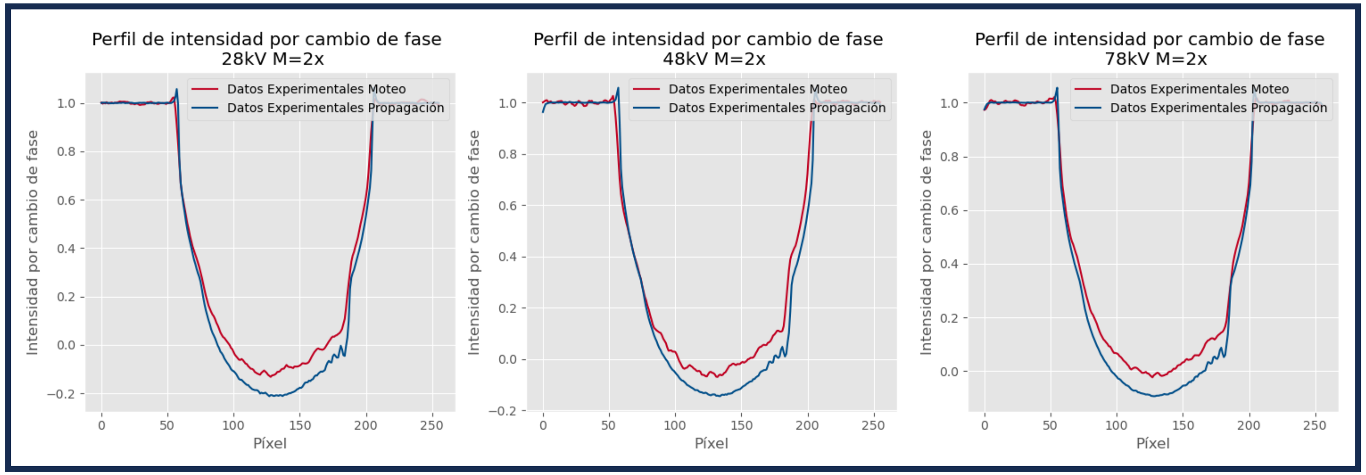

CNR Calculation

CNR	
Voltaje	Imágenes por propagación
28kV	0.77 ± 0.02
48kV	0.85 ± 0.02
78kV	1.18 ± 0.02

CNR imágenes filtradas	
Voltaje	Imágenes por moteo
28kV	0.8 ± 0.1
48kV	1.16 ± 0.08
78kV	1.17 ± 0.06

Experimental results: PMMA Phantom

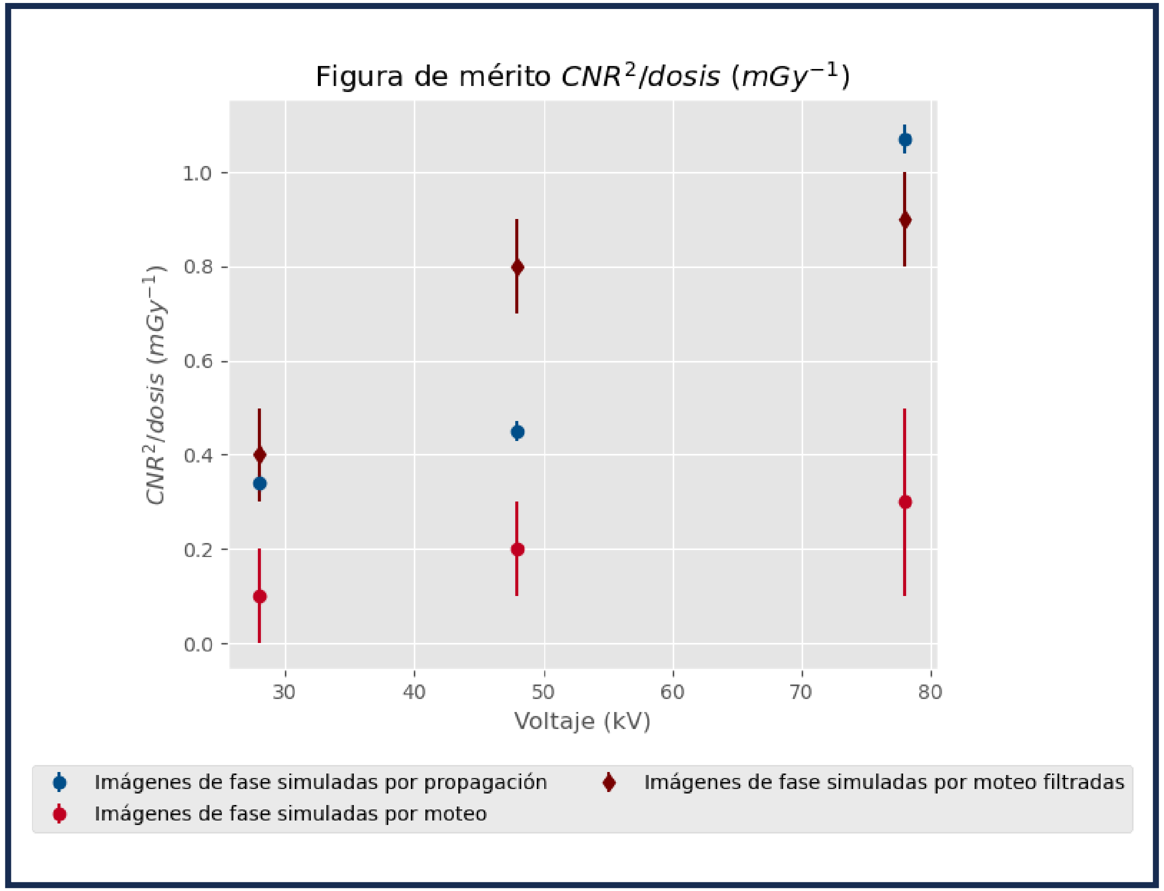

Applying a Gaussian filter is completely necesary for speckle to be a competitive technique

Figura de mérito $CNR^2/dosis$ (mGy^{-1})			
Voltaje	Propagación	Moteo	Moteo filtrada
28kV	0.34 ± 0.02	0.1 ± 0.1	0.4 ± 0.1
48kV	0.45 ± 0.02	0.2 ± 0.1	0.8 ± 0.1
78kV	1.07 ± 0.03	0.3 ± 0.2	0.9 ± 0.1

At 48 kV speckle provides 77.8% more visibility per absorbed dose than in-line

Experimental results: Pig Artery

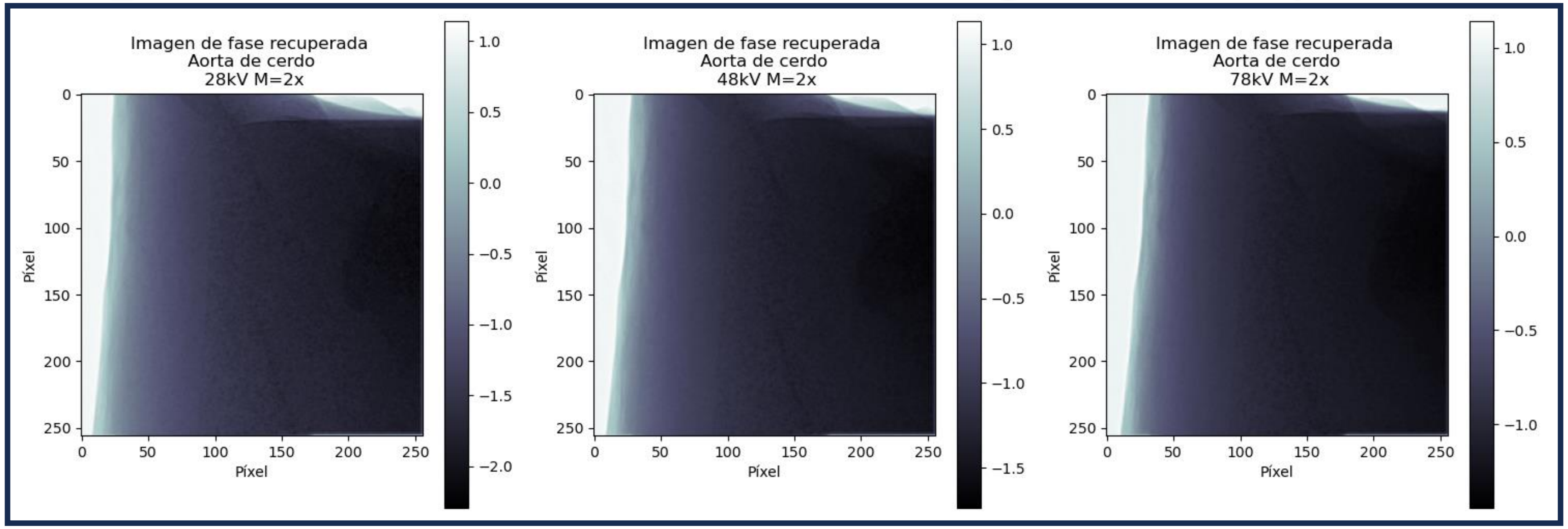

In-line

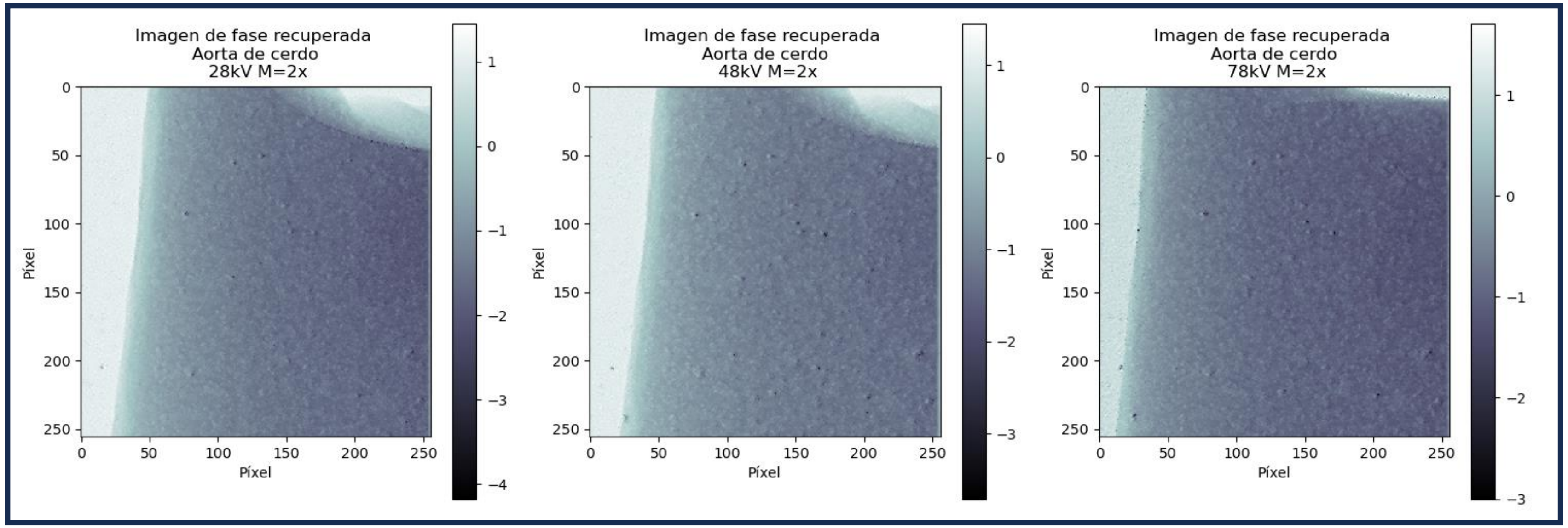

Speckle-based

Universidad de los Andes | Grupo de Investigación Altas Energías

Experimental results: Pig Artery

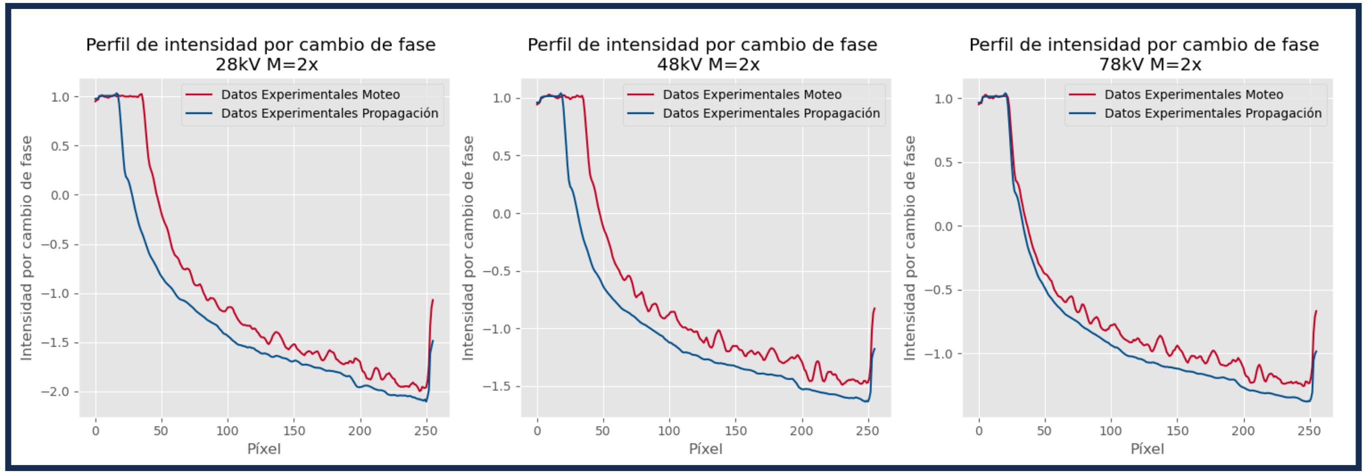

Gaussian filter applied.
We can see the plaque-blood interface near pixel 200.

CNR Calculation

CNR imágenes filtradas	
Voltaje	Imágenes por moteo
28kV	13 ± 4
48kV	8 ± 2
78kV	8 ± 1

CNR imágenes filtradas	
Voltaje	Imágenes por propagación
28kV	19.05 ± 0.05
48kV	31.51 ± 0.04
78kV	38.74 ± 0.04

The presence of artifacts in the speckle images affects the CNR regions and therefore decreases with energy.

Conclusions

- One phase image retrieved with MIST provides 12% more absorbed dose than one retrieved with Paganin algorithm. This means the main difference between techniques is CNR calculated on the atherosclerotic plaque.

- Statistical fluctuations is the major weakness of the speckle-based method.

- It is neecsary to implement a Gaussian filter to reduce noise in the retrieved images.

- As the phase recovery algorithms were implemented, the technique that offers the best image quality as a function of its dose is In-line PCI.

Future work

- We must make more precise measurements of the incident and absorbed radiation by the phantom at an experimental level, using technologies such as TIMEPIX detector and NOMEX dosimeter.

- Our results are highly dependent on the phase retrieval algorithm, we suggest employing other algorithms such as Beltrán (in-line) and UMPA or XSVT (speckle-based).

- We must explore the utility of Dark-field imaging in angiography.

- The δ/β ratio of blood has a maximum between 35keV and 40keV. It would be desirable to use an effective energy on the source near these energies to obtain a better visibility and in consecuece better image quality.

References

1. Constance, J. (2023, June 20). *What is angiography?*. News. https://www.news-medical.net/health/What-is-Angiography.aspx
2. L. Flors, K. Hagspiel, A. Park, P. Norton, and C. Leiva-Salinas, “Malformaciones vasculares y tumores de partes blandas. parte 2: lesiones de bajo flujo,” Radiología, vol. 61, no. 2, pp. 124–133, 2019.
3. C. L. Dumoulin and H. Hart Jr, “Magnetic resonance angiography.,” Radiology, vol. 161, no. 3, pp. 717–720, 1986.
4. M. Rafieian-Kopaei, M. Setorki, M. Doudi, A. Baradaran, and H. Nasri, “Atherosclerosis: process, indicators, risk factors and new hopes,” International journal of preventive medicine, vol. 5, no. 8, p. 927, 2014.
5. E. Falk, “Pathogenesis of atherosclerosis,” Journal of the American College of cardiology, vol. 47, no. 8S, pp. C7–C12, 2006.
6. Stanford Medicine. (2020, June 19). *Unregulated artery cell growth may drive atherosclerosis, Stanford Medicine Research shows*. News Center. https://med.stanford.edu/news/all-news/2020/06/unregulated-artery-cell-growth-may-drive-atherosclerosis.html
7. M. Endrizzi, “X-ray phase-contrast imaging,” Nuclear instruments and methods in physics research section A: Accelerators, spectrometers, detectors and associated equipment, vol. 878, pp. 88–98, 2018.
8. A. Bravin, P. Coan, and P. Suortti, “X-ray phase-contrast imaging: from pre-clinical applications towards clinics,” Physics in Medicine & Biology, vol. 58, no. 1, p. R1, 2012.
9. L. Brombal, X-ray phase-contrast tomography: Underlying Physics and Developments for Breast Imaging. Springer Nature, 2020.
10. A. V. Ávila, “Aplicación de la técnica de rayos x por contraste de fase para detección de lesiones mamarias,” Repositorio Institucional de la Universidad Distrital Francisco José de Caldas, 2019.
11. S. Tao, C. He, X. Hao, C. Kuang, and X. Liu, “Principles of different x-ray phase-contrast imaging: A review,” Applied Sciences, vol. 11, no. 7, p. 2971, 2021.
12. D. M. Paganin and D. Pelliccia, “Tutorials on x-ray phase contrast imaging: Some fundamentals and some conjectures on future developments,” arXiv preprint arXiv:1902.00364, 2019.
13. S.-A. Zhou and A. Brahme, “Development of phase-contrast x-ray imaging techniques and potential medical applications,” Physica Medica, vol. 24, no. 3, pp. 129–148, 2008.

References

14. S. J. Alloo, K. S. Morgan, D. M. Paganin, and K. M. Pavlov, “M ultimodal intrinsic speckletracking (mist) to extract images of rapidly varying diffuse x-ray dark-field,” Scientific
15. Reports, vol. 13, no. 1, p. 5424, 2023.R. Cerbino, L. Peverini, M. Potenza, A. Robert, P. Bösecke, and M. Giglio, “X-rayscattering information obtained from near-field speckle,” Nature Physics, vol. 4, no. 3, pp. 238–243, 2008.
16. M.-C. Zdora, “State of the art of x-ray speckle-based phase-contrast and dark-field imaging,” Journal of Imaging, vol. 4, no. 5, p. 60, 2018.
17. I. A. Aloisio, D. M. Paganin, C. A. Wright, and K. S. Morgan, “Exploring experimental parameter choice for rapid speckle-tracking phase-contrast x-ray imaging with a paper analyzer,” Journal of Synchrotron Radiation, vol. 22, no. 5, pp. 1279–1288, 2015.
18. M. Zdora, P. Thibault, C. Rau, and I. Zanette, “Characterisation of speckle-based x-ray phase-contrast imaging,” in Journal of Physics: Conference Series, vol. 849, p. 012024, IOP Publishing, 2017.
19. S. Berujon and E. Ziegler, “X-ray multimodal tomography using speckle-vector tracking,” Physical Review Applied, vol. 5, no. 4, p. 044014, 2016.
20. K. M. Pavlov, D. M. Paganin, H. T. Li, S. Berujon, H. Rougé-Labriet, and E. Brun, “X-ray multi-modal intrinsic-speckle-tracking,” Journal of Optics, vol. 22, no. 12, p. 125604, 2020.
21. S. J. Alloo, D. M. Paganin, K. S. Morgan, M. J. Kitchen, A. W. Stevenson, S. C. Mayo, H. T. Li, B. M. Kennedy, A. Maksimenko, J. C. Bowden, et al., “Dark-field tomography of an attenuating object using intrinsic x-ray speckle tracking,” Journal of Medical Imaging, vol. 9, no. 3, pp. 031502–031502, 2022.
22. Geant4 Collaboration, Introduction to geant4, 2023.
23. L. Brombal, F. Arfelli, F. Brun, F. Longo, N. Poles, and L. Rigon, “X-ray differential phase-contrast imaging simulations with geant4,” Journal of Physics D: Applied Physics, vol. 55, no. 4, p. 045102, 2021.
24. G. Poludniowski, A. Omar, R. Bujila, and P. Andreo, “Spekpy v2. 0—a software toolkit for modeling x-ray tube spectra,” Medical Physics, vol. 48, no. 7, pp. 3630–3637, 2021.
25. R. Bujila, A. Omar, and G. Poludniowski, “A validation of spekpy: A software toolkit for modelling x-ray tube spectra,” Physica Medica, vol. 75, pp. 44–54, 2020.

References

26. Hall EJ, Giaccia AJ. Radiobiology for the Radiologist. Lippincott Williams & Wilkins, Philadelphia, 2011.
27. Sabalza Castillejo, W. F. Determinación de la dosis absorbida en la zona cerebral a partir de imágenes de tomografía de emisión de positrones (Doctoral dissertation),2016.

Result analysis: CNR and Dose

We calculate CNR as $$CNR = \left| \frac{\overline{S}_{placa} - \overline{S}_{sangre}}{\sigma_{sangre}} \right|$$

Absorbed dose by a material is $$D = \frac{\Delta E}{\Delta M}$$ $$[D] = J/kg = Gy$$

To compare both tecniques we use $$F = \frac{CNR^2}{Dosis}$$

Experimentally we tried to measure kerma in air with NOMEX dosimeter

Medida Experimental

kerma por segundo ($\pm 0{,}001\ \mu Gy/s$)			
Voltaje	Ausencia de lija	Presencia de lija	Cociente
28kV	0.160	0.120	1.33
48kV	0.421	0.329	1.28
78kV	0.815	0.780	1.04

Medida Computacional

kerma			
Voltaje	Ausencia de lija ($\pm 0{,}2\ \mu Gy$)	Presencia de lija ($\pm 0{,}1\ \mu Gy$)	Cociente
28kV	58.9	31.2	1.88
48kV	52.8	29.4	1.79
78kV	42.4	24.4	1.74

NOMEX measurements are not accurate → We studied dose computationally → Absorbed dose

Photoelectric and Compton Effect Cross-sections

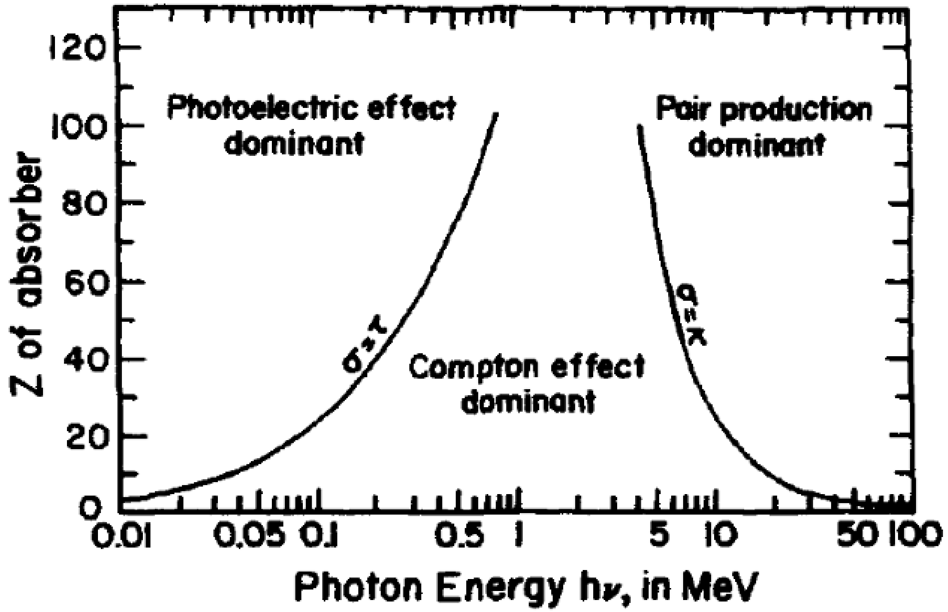

Fig 6. Relative importance between the effects that involve X-ray photons. Taken from [26].

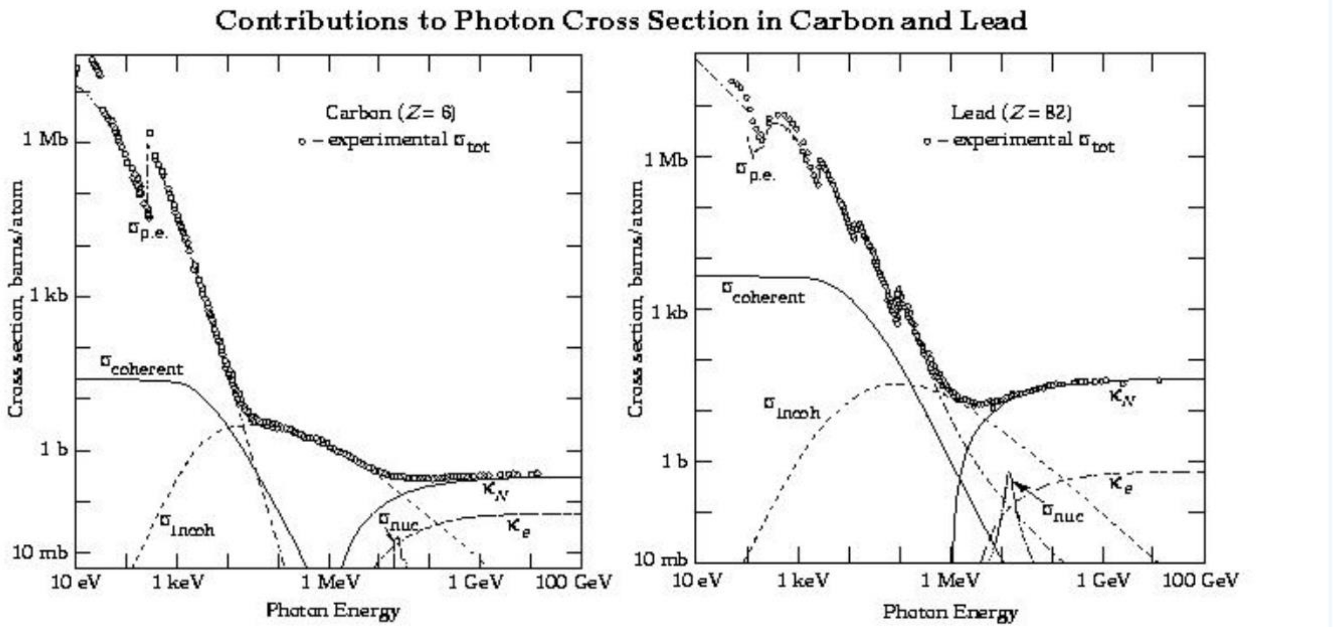

Fig 7. Cross-sections of the radiation-matter interactions. Taken from [27].

In our project the Photoelectric Effect domains over others in the energy range used ~7 keV

δ/β ratio as a function of energy

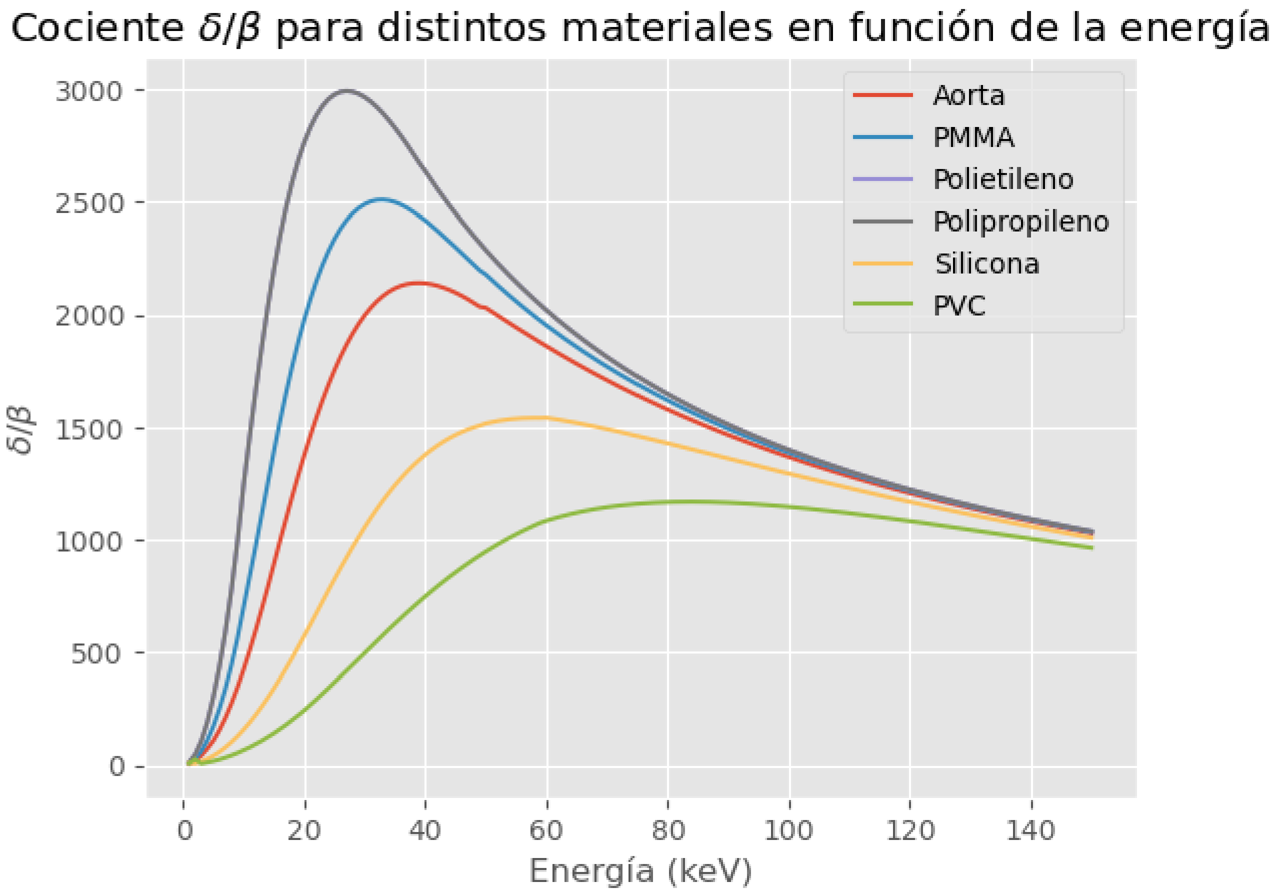

PMMA is the most physically suitable material to simulate blood vessels.

δ/β ratio of aorta and blood

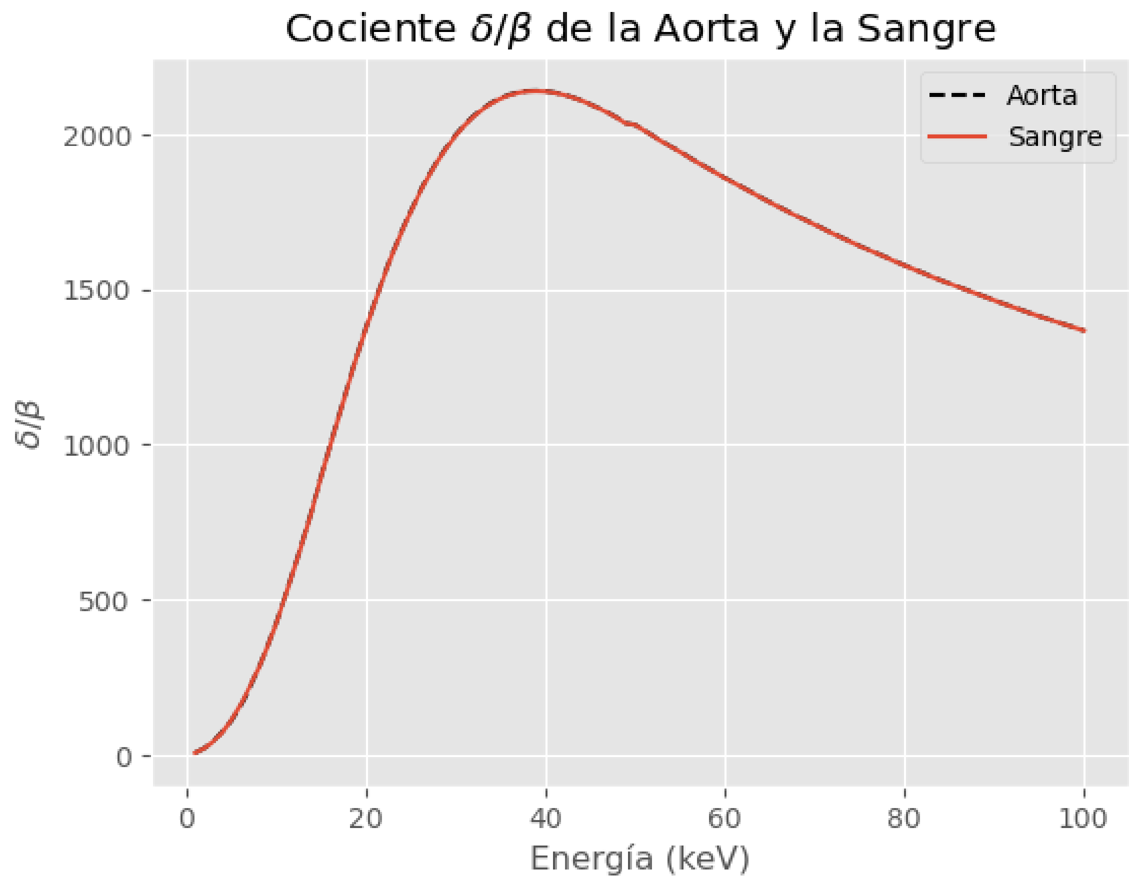

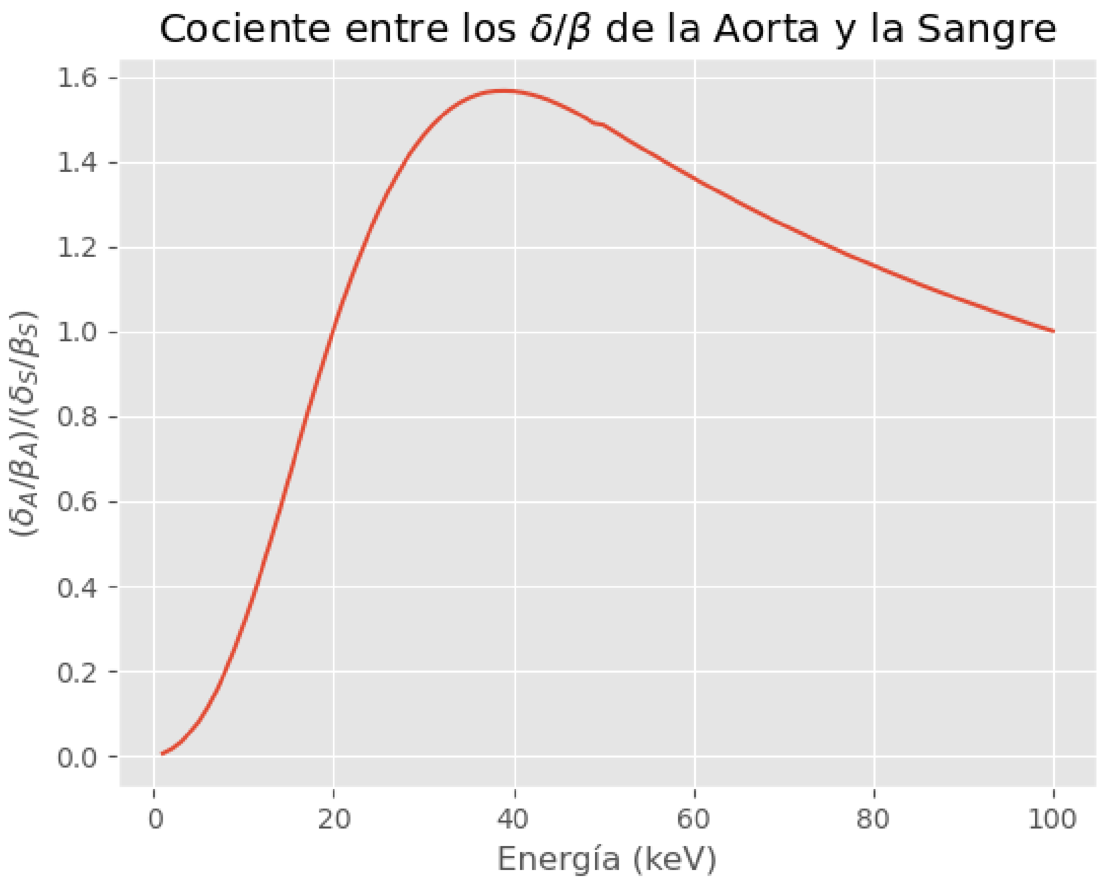

While it appears that the δ/β ratio is the same for blood and aorta, they differ subtly. This is sufficient to identify each material in a phase image.

Universidad de los Andes | Grupo de Investigación Altas Energías

Dark-field images

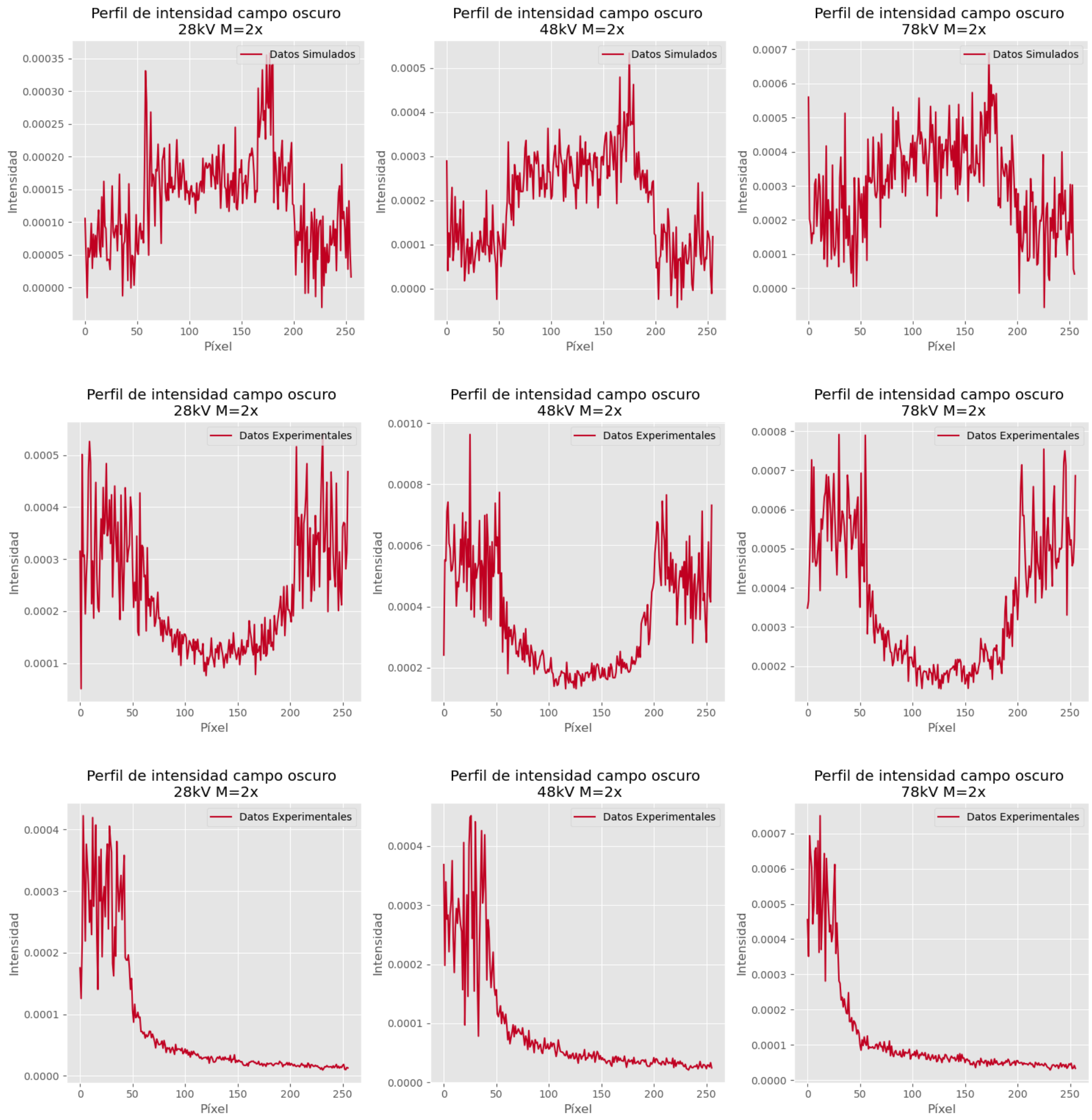

→ Simulations

→ PMMA Phantom

→ Pig artery

Due to the high attenuation of blood, darkfield images do not provide any additional information about structures that are not resolved by the detector.

V

Universidad de los Andes | Grupo de Investigación Altas Energías

Phase images: Computational simulations

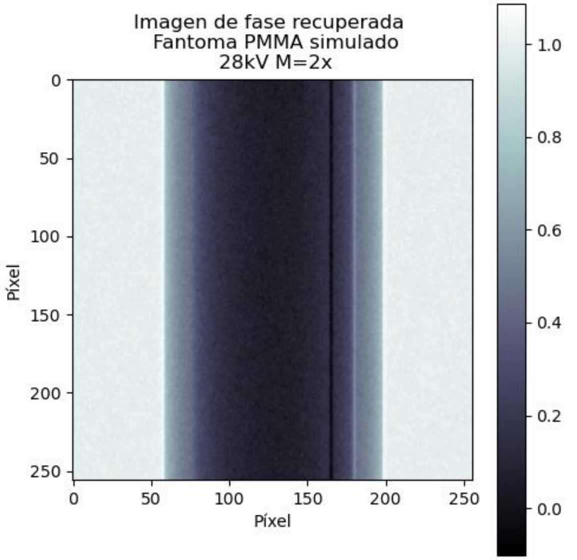

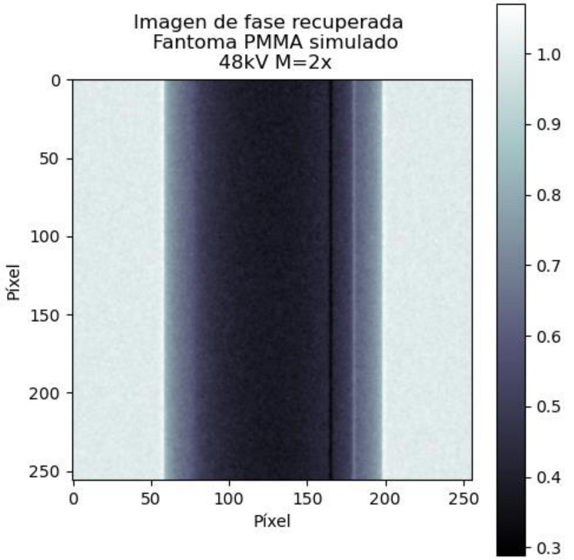

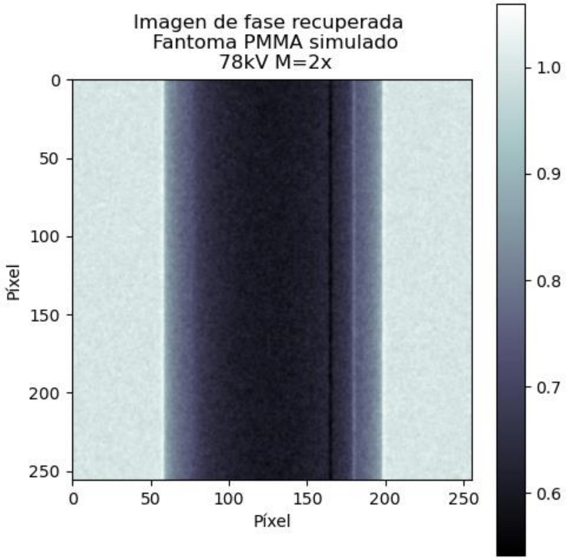

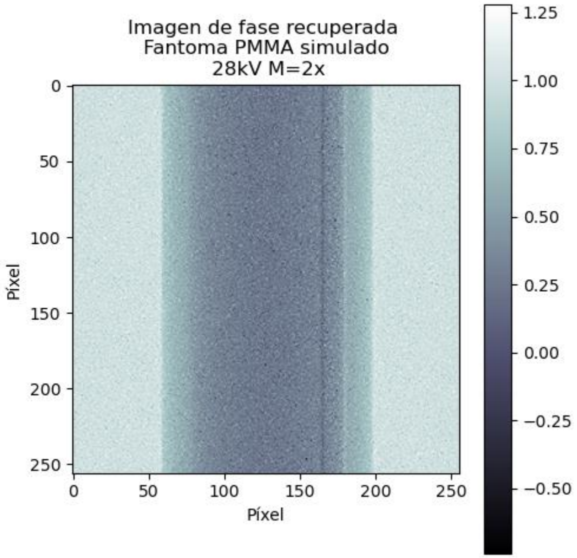

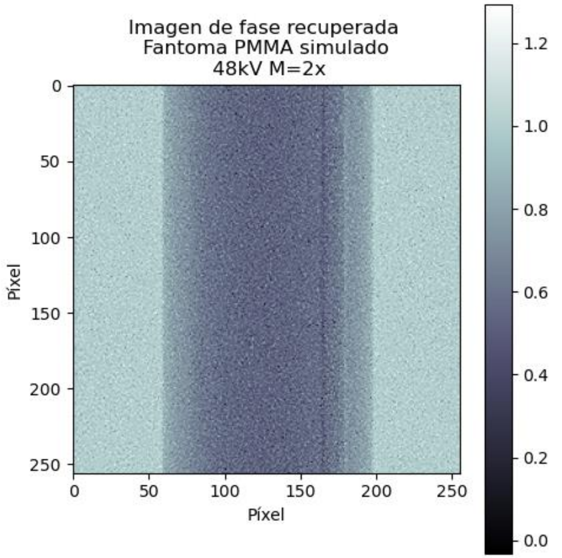

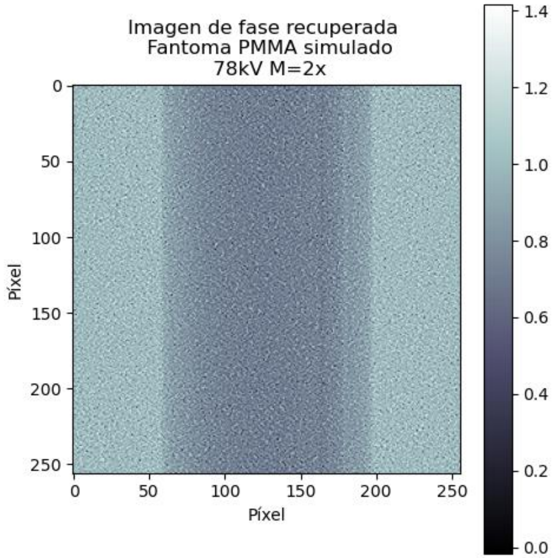

Phase images: Experimental images

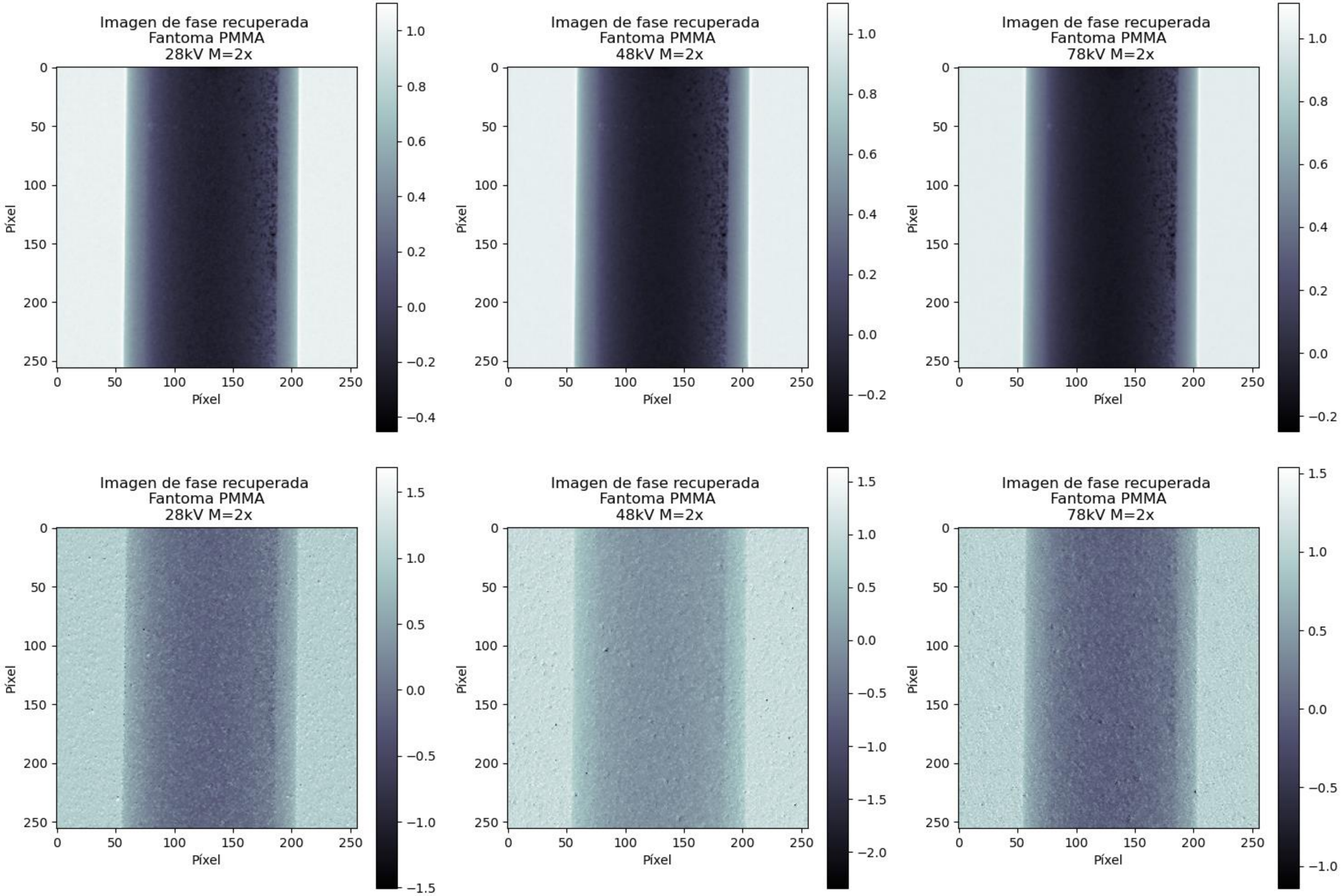

Universidad de los Andes | Grupo de Investigación Altas Energías

Phase-images: Filtered speckle-based images

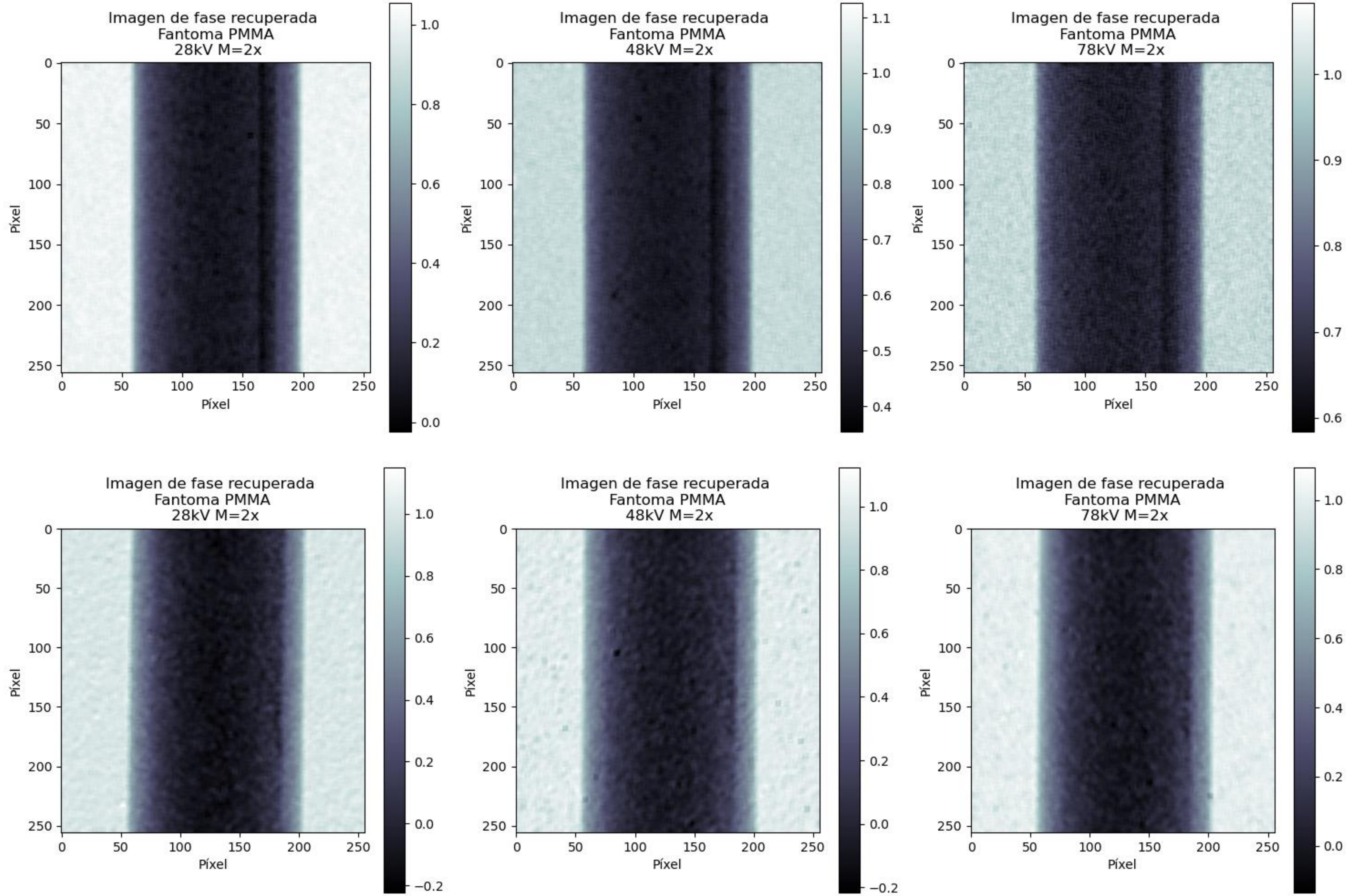

Phase-images: Filtered speckle-based images

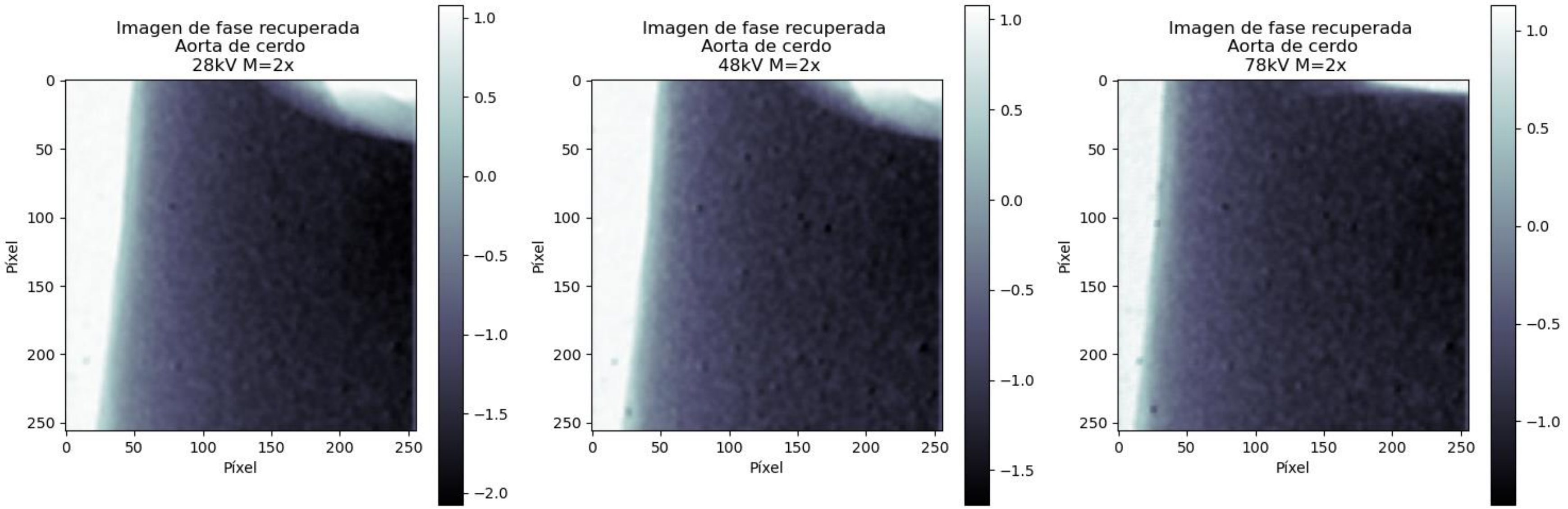

CNR Calculation: Regions of interest